18B.1

Synergy between Cloud Radar Polarimetry and Doppler Spectral Analysis in Ice and Mixed-Phase Clouds

Mariko Oue[1], Pavlos Kollias[1,2], Alexander Ryzhkov[3], and Edward P. Luke[2]

1. School of Marine and Atmospheric Sciences, Stony Brook University
2. Environmental and Climate Sciences Department, Brookhaven National Laboratory
3. Cooperative Institute for Mesoscale Meteorological Studies / National Severe Storms Laboratory

1. INTRODUCTION

Arctic clouds often include mixed-phase layers, which are defined as clouds in which supercooled liquid water droplets and solid ice crystals coexist at temperatures between -40°C and 0°C, and produce a variety of ice particle types in the same cloudy volume (Lebo et al. 2008; Karlsson and Svensson, 2011). Understanding ice microphysical processes in the Arctic is a challenge due to these complex interactions, making them difficult to accurately characterize from an observational viewpoint, and thus even more difficult to parameterize in models.

Collocated observations by millimeter-wavelength radars and polarization lidars have been used from space and the ground to identify the presence of embedded supercooled liquid layers in ice clouds by exploiting the sensitivity of lidars to their numerous liquid droplets and the sensitivity of radars to their fewer but larger ice particles. Advancing beyond the identification of mixed-phase clouds requires the use of multiparameter radar observations (e.g., Doppler spectra, multi-wavelength, and polarimetry). Profiling radar Doppler spectra offer the ability to identify and separate the liquid and ice radar returns (e.g., Shupe et al. 2004; Luke et al. 2010). In addition to radar Doppler spectra measurements, radar polarimetry can also offer the capability to identify ice hydrometeor species (e.g., Hall et al. 1984 among others) as well as their spatial distributions (e.g., Kumjian and Lombardo 2017 among others).

It is very common for different habits of ice particles to coexist in the radar resolution volume and it is impossible to separate and quantify their constituent amounts if a single radar variable such as radar reflectivity (Z_H) is utilized. Various ice habits contribute differently to Z_H, differential reflectivity (Z_{DR}), and specific differential phase (K_{DP}), and some segregation of different ice types within the radar resolution volume is possible if all three radar variables are analyzed (e.g., Schrom et al. 2015; Kumjian et al. 2016). Combining polarimetric measurements with the analysis of Doppler spectra yields a much better chance to identify and separate different types of ice and quantify their amounts (e.g., Moisseev et al. 2015).

Several previous studies have analyzed polarimetric signatures in ice regions observed in mid-latitude heavy-snow producing winter storms by longer-wavelength precipitation radars (i.e., operating at S and C bands). However, polarimetric radar analysis of Arctic clouds faces the challenge of lower ice water content and smaller ice particles compared to mid-latitude storms, resulting in low signal-to-noise ratio and weak K_{DP} signatures at longer radar wavelengths (Oue et al. 2016). The US Department of Energy Atmospheric Radiation Measurement (ARM) program operates an atmospheric observatory at Oliktok Point, Alaska (Mather and Voyles 2013), where profiling and scanning millimeter-wavelength radars provide unique multi-wavelength, polarimetric, and Doppler spectral measurements (Kollias et al. 2007, 2014). Herein, the benefit of combining time-versus-height fields of polarimetry and Doppler spectra is demonstrated in two key areas of the clouds where different ice particle types and cloud water may coexist: the dendritic growth layer (DGL) and the mixed-phase layer (MPL) beneath.

2. DATA AND METHOD

Data were collected by the ARM Mobile Facility at the Oliktok site instrumented with the Ka-band ARM Zenith pointing Radar (KAZR), Ka- and W-band 2nd generation Scanning ARM Cloud Radars (Ka/W-SACR2), ceilometer, microwave radiometer, and sounding equipment in the spring season in 2016.

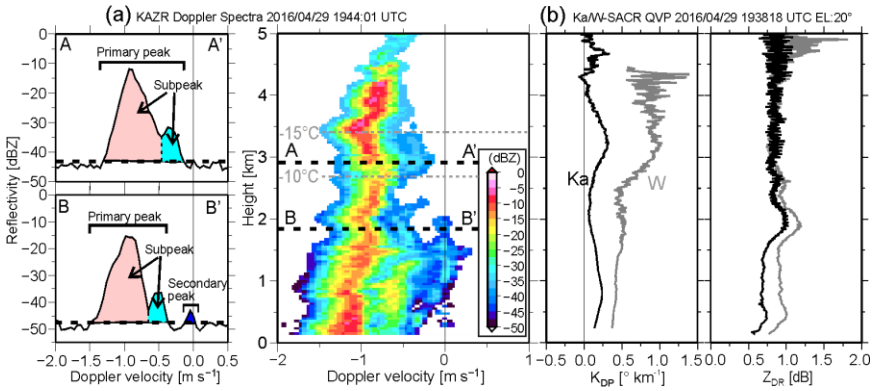

Figure 1: (a) Example of KAZR Doppler velocity spectra showing a profile and single spectrum along A-A' and B-B'. Color shade in the profile plot represents reflectivity. Horizontal gray dashed lines represent heights of temperature of -10°C and -15°C. (b) QVPs of Z_{DR} and K_{DP} estimated from a PPI scan at an elevation angle of 20°.

2.1. KAZR MICROARSCL

During the time period of this study, KAZR collected 256-point Doppler spectra with a temporal resolution of 2 seconds. The range spacing of KAZR is 30 m and the beam width is 0.33°. The recorded radar Doppler spectra are post-processed using the Microscale Active Remote Sensing of Clouds (MICROARSCL; Kollias et al., 2007; Luke et al. 2008) data product, which generates an objective analysis of the Doppler spectrum morphology by estimating a number of its shape parameters. Of interest to this study is the detection of multi-peak radar Doppler spectra, the decomposition of the radar Doppler spectrum into a primary peak and a secondary peak, and the estimation of the radar reflectivity and mean Doppler velocity separately for each peak. The primary peak is also decomposed into subpeaks, the reflectivity and mean Doppler velocity of which are calculated. The definition of these peaks is illustrated in Fig. 1a and described in section 2.3.

2.2. Ka/W-SACR2 Observations

The Ka/W-SACR2 radars perform polarimetric measurements through simultaneous transmission and simultaneous reception of horizontally and vertically polarized waves. The radars share the same pedestal and have different size antennas to ensure a matched beam width (0.32°) at the two radar wavelength. The range gate spacing for both radars is 30 m. Biases attributed to elevation angles in Z_{DR} and K_{DP} are corrected using theoretical formulas presented in Ryzhkov et al. (2005) and Schneebeli et al. (2013).

This study utilizes a Quasi-Vertical Profile (QVP) methodology (Ryzhkov et al. 2016) using SACR2 Plan Position Indicator (PPI) scans. The QVP technique employs azimuthal averaging of polarimetric radar variables from conical PPI scans at high elevations to produce quasi-vertical profiles of polarimetric radar variables in a height versus time format. We use PPI scans at an elevation angle of 20° every 3 minutes with a scan rate of 2° s^{-1}. Since the slant range resolution of the PPI data is 30 m, the corresponding vertical spacing is 10 m. The KAZR data were vertically interpolated into the QVP height grid to match the QVP and KAZR data. Because a single PPI scan takes 3 minutes for 360° in azimuth angles, all KAZR MICROARSCL data during 3 minutes corresponding to every SACR2 PPI are used.

2.3. Synergy Analysis

Multimodal radar Doppler spectra have been often used to infer the presence of mixed-phase conditions in deep precipitating ice clouds (e.g., Luke et al. 2010; Oue et al. 2015a,b). An example of multimodal spectra is shown in Fig. 1a. In ice precipitation clouds, total reflectivity is dominated by ice particles, which is shown as a primary peak in the Doppler spectrum (A-A'). The primary peak can have two subpeaks: the one associated with faster-falling particles which generally produce higher reflectivity (called the fast-falling subpeak hereafter) and the one attributed to slower-falling particles with lower reflectivity (called the slow-falling subpeak hereafter), implying that faster-falling particles have larger sizes and/or higher concentrations. Although

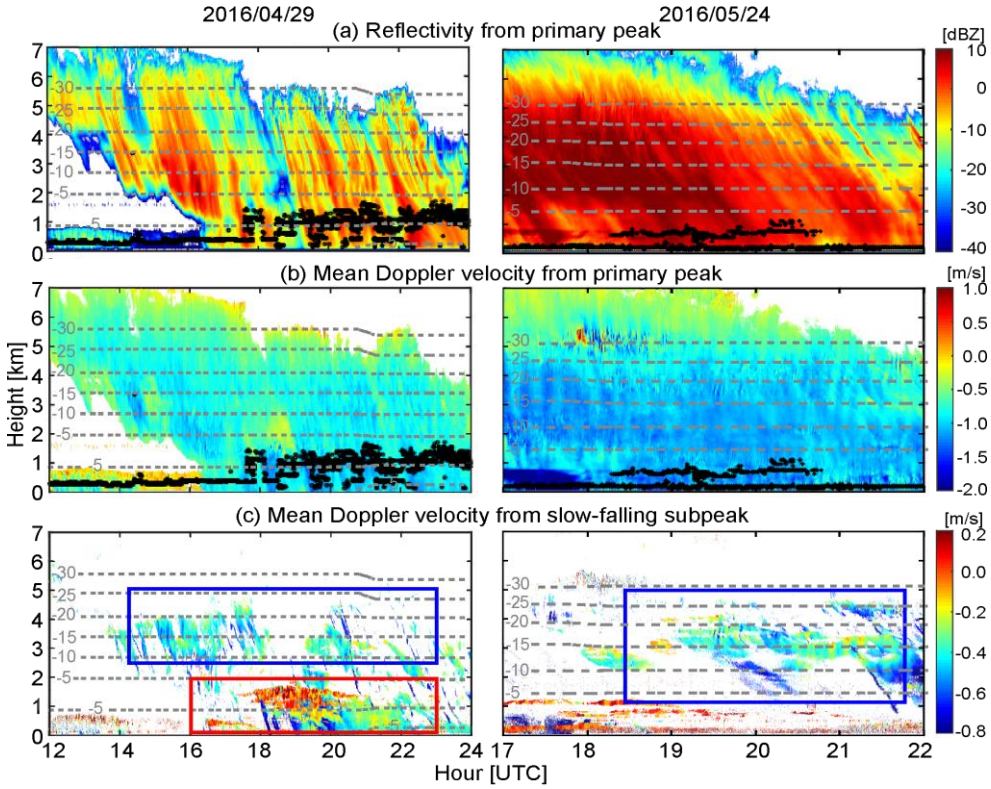

Figure 2: Time versus height cross sections of (a) KAZR reflectivity, (b) KAZR mean Doppler velocity, and (c) mean Doppler velocity from slow-falling subpeaks for April 29, 2016 (left column) and May 24, 2016 (right column). Boxes in (c) represent analysis regions used in Figs. 3 and 4 for the DGL (blue) and the MPL (red). Black dots in (a) and (b) represent ceilometer-observed cloud base heights indicating the presence of supercooled liquid layers. Gray dashed lines in (a-c) represent temperature from -25°C to -5°C with a 5°C increment from soundings at Oliktok.

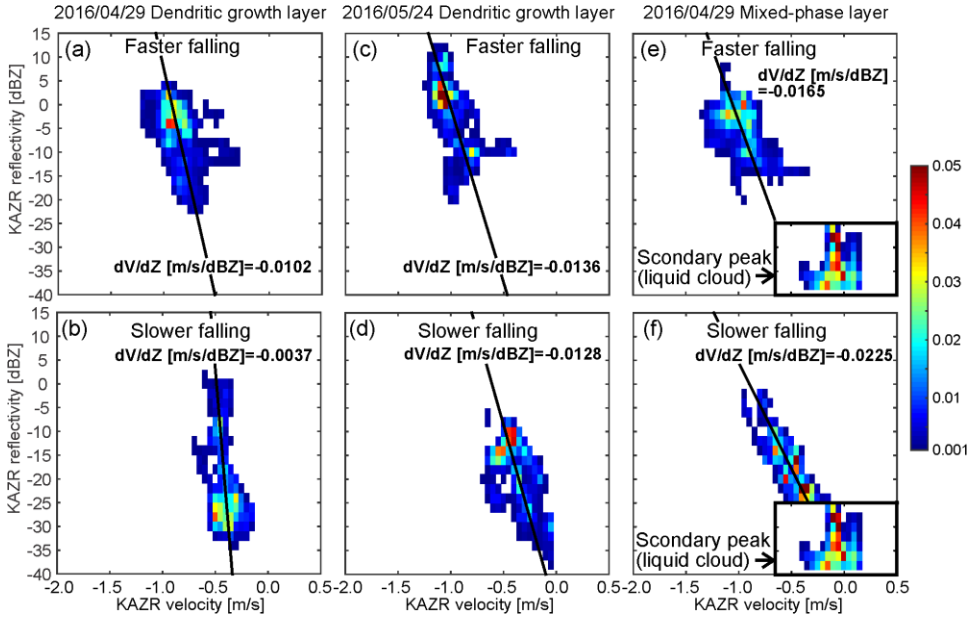

Figure 3: Probability density distributions of KAZR Doppler velocity versus KAZR reflectivity for the fast-falling subpeaks (top row) and slow-falling subpeaks (bottom row) for (a,b) the DGL of April 29 (blue box in Fig. 2c, left), (c,d) for the DGL of May 24, 2106 (blue box in Fig. 2c, right), and (e,f) the MPL of April 29, 2016 (red box in Fig. 2c, left). The linear least squares fit-ting lines and their slopes are presented in each panel. Same, but from the secondary peaks for the April 29 mixed-phased layer is overlapped in (e) and (f).

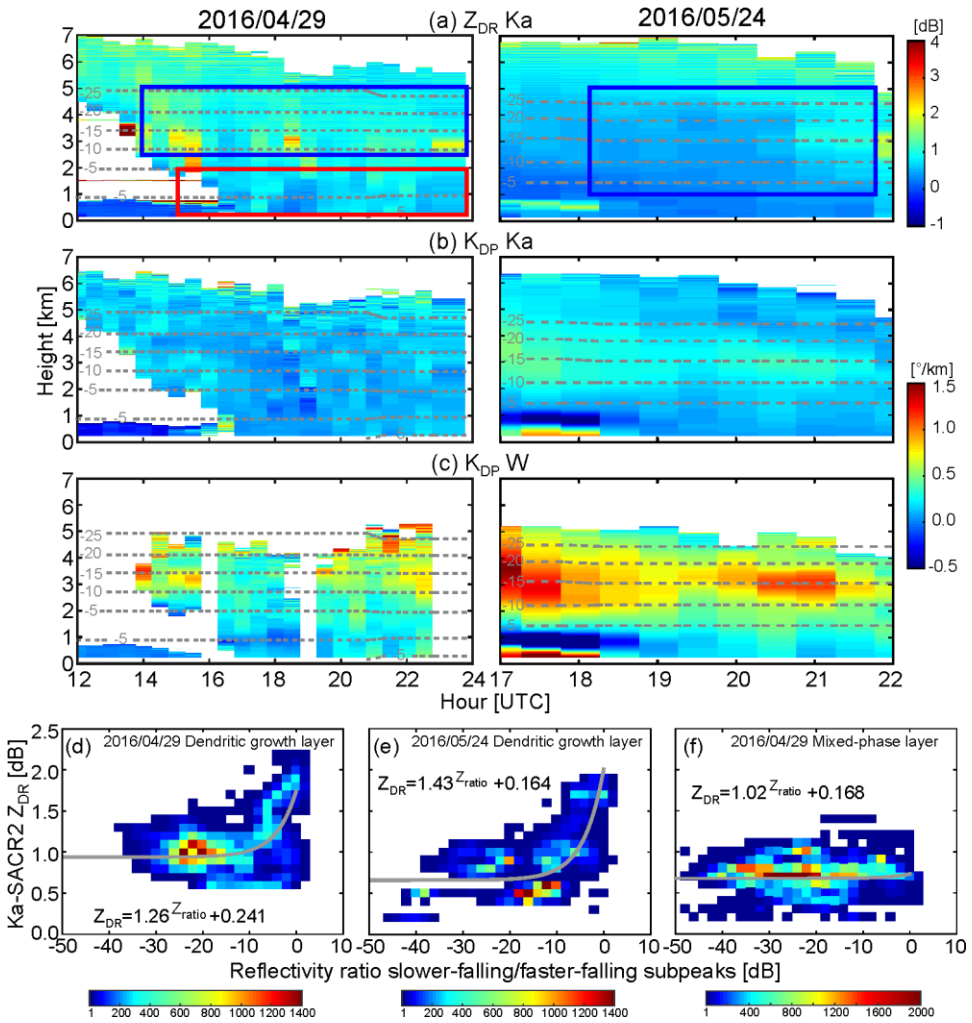

Figure 4: (Top to third rows): Time versus height cross sections of (a) Ka-SACR2 Z_{DR}, (b) Ka-SACR2 K_{DP}, and (c) W-SACR2 K_{DP} for April 29, 2016 (left column) and May 24, 2016 (right column). Gray dashed lines in (a-c) represent temperature from -25°C to -5°C with 5°C increment from soundings at Oliktok. (Bottom row): Reflectivity ratio of slow-falling subpeak to fast-falling subpeak (Z_{ratio}) versus Ka-SACR2 Z_{DR} plots for (d) the DGL of April 29, 2016 (blue box in Fig. 2c, left and in Fig. 4a, left), (e) the DGL of May 24, 2016 (blue box in Fig. 2c right and Fig. 4a right), and (f) the MPL of April 29, 2016 (red box in Fig. 2c left and Fig. 4a left). The best fit line (gray) and its equation are also shown in (d), (e), and (f). Z_{DR} and Z_{ratio} in the equations are in linear scale.

the fast-falling subpeak can produce weaker reflectivity when the particle number concentration is very low, this was not common during the spring season at the Oliktok site. Slow-falling subpeaks generally have downward mean Doppler velocity, suggesting falling ice particles rather than liquid ones. Liquid-cloud spectra commonly have mean Doppler velocity either near 0 m s^{-1} or slightly positive and low reflectivity (e.g., Rambukkange et al. 2011). Often, the cloud droplet Doppler spectrum is clearly separated from the ice spectrum (B-B', Fig. 1a). The QVPs of Ka/W-SACR2 Z_{DR} and K_{DP} corresponding to the KAZR Doppler spectra in Fig. 1a are shown in Fig. 1b. The magnitude of K_{DP} at both frequencies increases at around 3 km altitude near the center of the DGL, where the KAZR Doppler spectra show multi-modality, while Z_{DR} is relatively low. The low Z_{DR} values can be produced by large, more isotropic (quasi-isotropic) ice particles which dominate the total reflectivity. The higher K_{DP} values can be produced by anisotropic particles including quasi-isotropic (aspect ratios < 1) and slower-falling oblate particles. The contribution rates of these particles to K_{DP} values depend on number concentration (i.e. IWC).

3. RESULTS

Two deep precipitating ice events observed by the KAZR and the Ka/W-SACR2 on April 29 and May 24, 2016 are analyzed here. The time-height structure of the radar reflectivity and mean Doppler velocity of the KAZR Doppler spectra primary peak for the two cases are illustrated in Fig. 2a and 2b, respectively. The ceilometer cloud base detections are also shown indicating the presence of supercooled liquid layers. In addition, the mean Doppler velocity of the slow-falling sub-peak within the primary Doppler spectrum peak is shown in Fig. 2c. In the April 29 case, a significant fraction of the recorded radar Doppler spectra exhibits slower-falling subpeaks within a 2.5–4.5 km height and around the -15°C isotherm (DGL in this study). The slow-falling subpeaks have a significant downward value of Doppler velocity (0.3-0.8 m s^{-1}) suggesting slowly falling ice particles rather than liquid. Below 2 km height, slower-falling ice subpeaks are observed along with extensive horizontal layers where the slower-falling subpeaks have Doppler velocities around 0 m s^{-1} indicating the presence of supercooled liquid layers, defined as mixed-phase layers or MPL. This is further supported by the ceilometer detected cloud bases (Figs. 2a and 2b, in the left column). Slow-falling subpeaks with an ice signature (Doppler velocity 0.3-1.0 m s^{-1}) are also shown in the May 24 case at altitudes around -15°C from 1800 UTC to 2200 UTC. Below 1 km, slow-falling subpeaks with Doppler velocities around 0.0 m s^{-1} are observed, but no slowly-falling ice subpeaks exist in the low levels. In the rest of this section, emphasis is given to the DGL (for both cases, blue boxes in Fig. 2c) and MPL (for the April 29 case, red box in Fig. 2c).

3.1. Dendritic Growth Layer (DGL)

The frequency distributions of mean Doppler velocity versus radar reflectivity for the fast- and slow-falling Doppler spectra subpeaks in the two DGLs are shown in Figs. 3a-d. The downward velocity increases with reflectivity in both subpeak populations and the gradient of the mean Doppler velocity with radar reflectivity dV/dZ has values between 0.4-1.4 cm s^{-1} dB^{-1}. Small dV/dZ values are consistent with the presence of low density large particles. Considering the lack of a supercooled liquid layer in this regime, the ice particles can only grow via deposition and aggregation. In the DGL, lower dV/dZ values are observed during the April 29 case compared to the May 24 case, suggesting that heavier aggregation occurred during the May 24 case, and that light aggregation and/or depositional growth characterized the April 29 case.

Next, the SACR2 QVP K_{DP} measurements that correspond to the observed DGLs in the two cases are examined. Figure 4 shows height-versus-time plots of QVPs of the Ka-SACR2 Z_{DR} and K_{DP} and the W-SACR2 K_{DP}. Previous studies have indicated evidence of an increase in K_{DP} in a DGL around a temperature of -15°C (e.g., Kennedy and Rutledge 2011). A similar increase in K_{DP} is observed in both Ka/W-SACR2 observations through the selected periods for the April 29 and May 24 cases, but enhancement of the Ka-SACR2 K_{DP} on April 29 is weaker. The K_{DP} enhancement is roughly collocated in height with multimodal spectra shown as slow-falling subpeaks in Fig. 2c. Z_{DR} values observed during the April 29 case slightly increased in the DGL. For the May 24 case, observed Z_{DR} decreased downward while KAZR reflectivity and downward velocity increased (Figs. 2a and 2b). If it is assumed that the observed K_{DP} values in the DGL were produced by highly non-spherical ice particles such as dendrites or hexagonal plates, and such particles dominated ice in the cloud, then the expected Z_{DR} values should be much higher than the observed Z_{DR} values (i.e., greater than approximately 4 dB, e.g. Westbrook 2014). The observed Z_{DR} and K_{DP} values suggest that at least two types of ice particles coexisted in the multimodal spectra regions and that these had different contributions to Z_{DR} and K_{DP}. Large and more isotropic particles (quasi-isotropic), such as irregular or aggregated ice usually produce low Z_{DR} (e.g., Korolev and Isaac 2003). However, these quasi-isotropic ice particles (aspect ratios < 1) can produce tangible K_{DP} if their concentration is sufficiently high. Additional increase of K_{DP} can be attributed to plate-like crystals like dendrites or hexagonal plates which start growing locally at the DGL. Plate-like crystals have very high intrinsic Z_{DR} but the total Z_{DR} can be quite low if plate-like crystals are mixed with quasi-spherical ice particles in much higher concentration.

To quantify the extent to which smaller particles contribute to Z_{DR} in the multimodal Doppler spectra cases, the ratio of radar reflectivities associated with

the fast-falling subpeaks and slow-falling subpeaks versus Z_{DR} is shown in Figs. 4d and 4e. In the DGLs, Z_{DR} tended to increase when reflectivities from slow-falling subpeaks approached those from fast-falling subpeaks. This result supports the suggestion that plate-like slow-falling particles have more oblate shapes than quasi-isotropic ones; the plate-like particles could contribute more to the observed Z_{DR} when their reflectivity relative to the faster-falling particle reflectivity increased.

3.2 Mixed-Phase Layer (MPL)

One of the distinct differences of the MPL from the DGL is a larger gradient in the velocity-reflectivity relationship (approximately 2 cm s^{-1} dB^{-1}, Figs. 3e and 3f) for both slow- and fast-falling Doppler spectra subpeaks. The larger gradient indicates that the particles have faster fall velocity at a given reflectivity, suggesting compact, high-density particles. The Doppler spectra in this layer reveal a liquid cloud signature in slow-falling subpeaks and secondary peaks, which have near 0.0 m s^{-1} velocity (mostly greater than -0.3 m s^{-1}) and low reflectivity (less than -25 dBZ). The probability density distributions of KAZR Doppler velocity versus KAZR reflectivity from the secondary peak is combined in Fig. 3e and Fig. 3f. The ice particles could be effectively produced via growth by riming in the MPL.

Compared with the DGL, K_{DP} values from the MPL are lower; most of the values are close to 0.0° km^{-1} in Fig. 4b. This difference is clearly obvious at W band (Fig. 4c). The MPL also showed slightly lower Z_{DR}. These K_{DP} and Z_{DR} values suggest that the primary peaks were composed of isotropic particles in fast- and slow-falling subpeaks. The reflectivity ratio of slow-falling subpeaks to fast-falling subpeaks versus Ka-SACR Z_{DR} in the mixed-phase layer generally shows low Z_{DR} regardless of reflectivity ratio (Fig. 4f). This plot indicates that low-Z_{DR} particles, such as compact, more isotropic particles, dominated in both fast-falling and slow-falling subpeaks.

4 SUMMARY

The study of Arctic ice and mixed-phase clouds using millimeter-wavelength radars is an area of active and challenging research. The challenge arises from several factors including a great natural variability in the observed ice particle properties (mass, density, shape), the variability of their particle size distributions, the complexity of ice and mixed-phase microphysical processes, and uncertainties in the estimation of particle scattering properties. Multi-parameter (power, Doppler, polarization) radar observations have the best chance to improve our qualitative and quantitative understanding of ice and mixed-phase processes. The profiling and scanning millimeter-wavelength radars at the ARM Oliktok site provide such observations well matched in time and space. The results presented in this study illustrate the frequent occurrence of multimodal radar Doppler spectra in the DGL. Considering that multimodality in Doppler spectra requires particle populations well separated in fall velocity, it is conceivable that the velocity separation is produced by the dendritic growth of plate-like particles in this temperature range. Another area favoring the occurrence of multimodal Doppler spectra is the MPL. A key point illustrated in this study is that the careful comparison of the Doppler spectra peak properties (power, velocity) with the radar polarimetric variables can improve the interpretation of the radar measurements. The combination of radar Doppler spectra and radar polarimetric observations improves the identification of ice particles and their characteristics such as shape and fall speed through comparison of KAZR Doppler spectra and Ka/W-SACR2 QVP output at the same height. To understand formation and growth processes of these ice particles, wind shear and time evolution should be considered (e.g., Kalesse et al. 2016). The presented study introduces a new approach in analyzing ice and mixed-phase microphysics using the combination of radar Doppler spectra and polarimetric observations. Finally, the study is far from comprehensive; rather, it introduces only some of the many possible applications for which radar Doppler spectra and polarimetric measurements are available.

ACKNOWLEDGEMENTS

This research was supported by the Atmospheric System Research program of the Office of Biological and Environmental Research of the U.S. Department of Energy through grant DE-SC0014295 and contract DE-SC00112704. Data

used here were obtained from the ARM Climate Research Facility of the U.S. Department of Energy.

REFERENCES

Hall, M. P. M., J. W. F. Goddard, and S. M. Cherry (1984), Identification of hydrometeors and other targets by dual-polarization radar, *Radio Sci*., **19**, 132–140.

Kalesse, H., W. Szyrmer, S. Kneifel, P. Kollias, and E. Luke (2016), Fingerprints of a riming event on cloud radar Doppler spectra: observations and modeling, *Atmos. Chem. Phys*., **16**, 2997-3012.

Karlsson, J., and G. Svensson (2011), The simulation of Arctic clouds and their influence on the winter surface temperature in present-day climate in the CMIP3 multi-model dataset, *Climate Dyn*., **36**, 623–635.

Kennedy, P. C., and S. A. Rutledge (2011), S-band dual-polarization radar observations of winter storms. *J. Appl. Meteor. Climatol*., **50**, 844–858.

Kollias, P., N. Bharadwaj, K. Widener, I. Jo, and K. Johnson (2014), Scanning ARM cloud radars. Part I: Operational sampling strategies. *J. Atmos. Oceanic Technol*., **31**, 569–582.

Kollias, P., E. E. Clothiaux, M. A. Miller, E. P. Luke, K. L. Johnson, K. P. Moran, K. B. Widener, and B. A. Albrecht (2007), The Atmospheric Radiation Measurement Program cloud profiling radars: Second-generation sampling strategies, processing, and cloud data products. *J. Atmos. Oceanic Technol*., **24**, 1199–1214.

Korolev, A., and G. Isaac, 2003: Roundness and aspect ratio of particles in ice clouds. *J. Atmos. Sci.*, **60**, 1795 – 1808.

Kumjian, M. R., and K. A. Lombardo (2017), Insights into the evolving microphysical and kinematic structure of Northeastern U.S. winter storms from dual-polarization Doppler radar. *Mon. Wea. Rev*. **145**, 1033-1061.

Kumjian, M. R., S. Mishra, S. E. Giangrande, T. Toto, A. V. Ryzhkov, and A. Bansemer (2016), Polarimetric radar and aircraft observations of saggy bright bands during MC3E, *J. Geophys. Res. Atmos*., **121**, 3584–3607.

Lebo, Z. J., N. C. Johnson, and J. Y. Harrington (2008), Radiative influences on ice crystal and droplet growth within mixed–phase stratus clouds, *J. Geophys. Res*., **113**, D09203.

Luke, E., P. Kollias, K.L. Johnson, and E. E. Clothiaux (2008), A Technique for the Automatic Detection of Insect Clutter in Cloud Radar Returns. *J. Atmos. Oceanic Technol*., **25**, 1498-1513.

Luke, E., P. Kollias, and M. D. Shupe (2010), Detection of supercooled liquid in mixed-phase clouds using radar Doppler spectra, *J. Geophys. Res*., **115**, D19201.

Mather, J. H., and J. W. Voyles (2013), The Arm Climate Research Facility: A review of structure and capabilities, *Bull. Amer. Meteor. Soc*., **94**, 377–392.

Moisseev, D. N., S. Lautaportti, J. Tyynela, and S. Lim (2015), Dual-polarization radar signatures in snowstorms: Role of snowflake aggregation. *J. Geophys. Res. Atmos*., **120**, 12644–12655.

Oue, M., M. R. Kumjian, Y. Lu, J. Verlinde, K. Aydin, and E. E. Clothiaux (2015a), Linear depolarization ratios of columnar ice crystals in a deep precipitating system over the Arctic observed by zenith-pointing Ka-band Doppler radar. *J. Appl. Meteor. Climatol*., **54**, 1060-1068.

Oue, M., M. R. Kumjian, Y. Lu, Z. Jiang, E. E. Clothiaux, J. Verlinde, and K. Aydin (2015b), X-band polarimetric and Ka-band Doppler spectral radar observations of a graupel-producing Arctic mixed-phase cloud. *J. Appl. Meteor. Climatol*., **54**, 1335-1351.

Oue, M., M. Galletti, J. Verlinde, A. Ryzhkov, and Y. Lu (2016), Use of X-Band differential reflectivity measurements to study shallow Arctic mixed-phase clouds. *J. Appl. Meteor. Climatol*., **55**, 403-424.

Rambukkange, M. P., J. Verlinde, E. W. Eloranta, C. J. Flynn, and E. E. Clothiaux (2011), Using Doppler spectra to separate hydrometeor populations and analyze ice precipitation in multilayered mixed-phase clouds*. Geosci. Remote Sens. Lett. IEEE*, **8**, 108–112.

Ryzhkov, A. V., S. E. Giangrande, V. M. Melnikov, and T. J. Schuur, (2005), Calibration issues of dual-polarization radar measurements. *J. Atmos. Oceanic Technol*., **22**, 1138–1155.

Ryzhkov, A. V., P. Zhang, H. D. Reeves, M. R. Kumjian, T. Tschallener, S. Trömel, and C. Simmer, (2016), Quasi-vertical profiles – A new way to look at polarimetric radar data. *J. Atmos. Oceanic Technol.*, **33**, 551-562.

Schneebeli, M., N. Dawes, M. Lehning, and A. Berne (2013), High-resolution vertical profiles of X-band polarimetric radar observables during snowfall in the Swiss Alps. *J. Appl. Meteor. and Climatol.*, **52**, 378-394.

Schrom, R. S., M. R. Kumjian, and Y. Lu (2015), Polarimetric radar signatures of dendritic growth zones within Colorado winter storms. *J. Appl. Meteor. Climatol*., **54**, 2365-2388.

Shupe, M., P. Kollias, S. Y. Matrosov, and T. L. Schneider (2004), Deriving mixed-phase cloud properties from Doppler radar spectra*, J. Atmos. Ocean. Tech*., **21**, 660-670.

Westbrook, C. D. (2014), Rayleigh scattering by hexagonal ice crystals and the interpretation of dual-polarization radar measurements. *Quart. J. Roy. Meteor. Soc*., **140**, 2090–2096.